Important Notice to Authors

Attached is a PDF proof of your forthcoming article in PRE. Your article has 7 pages and the Accession Code is **EA10916**.

Please note that as part of the production process, APS converts all articles, regardless of their original source, into standardized XML that in turn is used to create the PDF and online versions of the article as well as to populate third-party systems such as Portico, CrossRef, and Web of Science. We share our authors' high expectations for the fidelity of the conversion into XML and for the accuracy and appearance of the final, formatted PDF. This process works exceptionally well for the vast majority of articles; however, please check carefully all key elements of your PDF proof, particularly any equations or tables.

Figures submitted electronically as separate PostScript files containing color usually appear in color in the online journal. However, all figures will appear as grayscale images in the print journal unless the color figure charges have been paid in advance, in accordance with our policy for color in print (http://publish.aps.org/authors/color-figures-print) and the relevant figure captions read "Color". For figures that will be color online but grayscale in print, please ensure that the text and captions clearly describe the figures to readers who view the article only in grayscale.

No further publication processing will occur until we receive your response to this proof.

Specific Questions and Comments to Address for This Paper

INSTRUCTIONS TO AUTHOR: Please make sure that color online figures can also be understood in the printed black-and-white version. Modify figures and/or captions if needed.

1 Please check new punctuation for the caption to Fig. 4; as meant? please amend as necessary.
2 Ref. 1: please update and complete as per style.
3 Refs. [9–12]: please verify volume and page numbers; please provide both.
4 Ref. 14: please provide publisher and city as per style.
5 Ref. 20: "Indiana" as meant?
6 Ref. 23: please update if possible.
Q: This reference could not be uniquely identified due to incomplete information or improper format. Please check all information and amend if applicable.

Other Items to Check

- Please note that the original manuscript has been converted to XML prior to the creation of the PDF proof, as described above. Please carefully check all key elements of the paper, particularly the equations and tabular data.
- Please check PACS numbers. More information on PACS numbers is available online at http://publish.aps.org/PACS/.
- Title: Please check; be mindful that the title may have been changed during the peer review process.
- Author list: Please make sure all authors are presented, in the appropriate order, and that all names are spelled correctly.
- Please make sure you have inserted a byline footnote containing the email address for the corresponding author, if desired. Please note that this is not inserted automatically by this journal.
- Affiliations: Please check to be sure the institution names are spelled correctly and attributed to the appropriate author(s).
- Receipt date: Please confirm accuracy.
- Acknowledgments: Please be sure to appropriately acknowledge all funding sources.
- Please check that your figures are accurate and sized properly. Make sure all labeling is sufficiently legible. Figure quality in this proof is representative of the quality to be used in the online journal. To achieve manageable file size for online delivery, some compression and downsampling of figures may have occurred. Fine details may have become somewhat fuzzy, especially in color figures. The print journal uses files of higher resolution and therefore details may be sharper in print. Figures to be published in color online will appear in color on these proofs if viewed on a color monitor or printed on a color printer.
- ***Overall, please proofread the entire article very carefully.***

Ways to Respond

- ***Web:*** If you accessed this proof online, follow the instructions on the web page to submit corrections.
- ***Email:*** Send corrections to preproofs@aptaracorp.com
  Subject: **EA10916** proof corrections
- ***Fax:*** Return this proof with corrections to +1.703.791.1217. Write **Attention:** PRE Project Manager and the Article ID, **EA10916**, on the proof copy unless it is already printed on your proof printout.

- ***Mail:*** Return this proof with corrections to **Attention:** PRE Project Manager, Physical Review E, c/o Aptara, 3110 Fairview Park Drive, Suite #900, Falls Church, VA 22042-4534, USA.

PHYSICAL REVIEW E **00**, 002800 (2013)

Density-feedback control in traffic and transport far from equilibrium

Marko Woelki*
Institute of Transportation Systems, German Aerospace Center, Rutherfordstraße 2, 12489 Berlin, Germany
(Received 7 January 2013; published xxxxx)

A bottleneck situation in one-lane traffic flow is typically modelled with a constant demand of entering cars. However, in practice this demand may depend on the density of cars in the bottleneck. The present paper studies a simple bimodal realization of this mechanism to which we refer to as density-feedback control (DFC): If the actual density in the bottleneck is above a certain threshold, the reservoir density of possibly entering cars is reduced to a different constant value. By numerical solution of the discretized viscid Burgers equation a rich stationary phase diagram is found. In order to maximize the flow, which is the goal of typical traffic-management strategies, we find the optimal choice of the threshold. Analytical results are verified by computer simulations of the microscopic totally asymmetric exclusion process with DFC.

DOI: 10.1103/PhysRevE.00.002800 PACS number(s): 89.40.−a, 05.40.−a, 05.70.Ln, 02.50.−r

I. INTRODUCTION

In the physical literature, traffic flow is modelled from different viewpoints as hydrodynamic models (on a macroscopic scale) or microscopic stochastic models. Microscopic approaches usually can be considered as a generalization of the so-called totally asymmetric exclusion process (TASEP). The model is defined on a discrete one-dimensional lattice that represents the road. Each lattice site can either be empty or occupied by exactly one particle (car). If the site in front is empty, cars move to the next site at a certain rate or probability depending on the dynamics (either random-sequential or parallel). This process is widely studied mathematically and due to its exact solvability it is of great interest for nonequilibrium statistical physics; see Ref. [1] for a recent review. Of particular mathematical interest is the model with open boundaries, where particles may enter the first site at rate α and leave the last site at rate β that differs from the bulk-hopping rate in general. Depending on the values of those parameters one finds that the system can be in either of three phases, a low-density phase, a high-density phase, or a maximum-current phase. For traffic applications one often uses a parallel update instead of the generic random-sequential update studied here. Note that if cars are allowed to move further than a single site under such a parallel update scheme this leads to the so-called Nagel-Schreckenberg model [2]. On the other hand, the macroscopic approaches are typically based on investigations of Lighthill and Witham [3], who described the effect of moving traffic jams by traveling-wave solutions of a simple partial differential equation. Since this inital work, there have been a number of generalizations of the hydrodynamic approach [4,5]. For example, the viscid Burgers equation is a generalization of the Lighthill-Witham equation with an additional diffusive term. This modification is enough to describe qualitatively on a hydrodynamic Eulerian scale the TASEP phase diagram; see Ref. [6] for further references. By discretization of space, the Burgers equation recovers the mean-field equations of the TASEP in which correlations between neighboring sites of the lattice are neglected [7].

The present paper models a road section to which cars can enter at the left end and leave at the right end. Common physical approaches of microscopic and macroscopic models assume a constant demand for entering the lattice. In the TASEP this is reflected by a constant rate α at which a particle enters the first lattice site if it is empty. From the viewpoint of the Burgers equation this corresponds to a constant left reservoir density $\rho_l = \alpha$ of customers. This fact will be changed in our investigations; see Refs. [8–11] for related approaches. One way to think about it is to assume that those customers have a route alternative [12–14] and that they can anticipate the density of cars on the road section, and then a fraction of those customers will take an alternative if the density ρ exceeds a certain threshold ρ^*. Thus, the density of potential customers is reduced from $\rho_l = \rho_-$ to $\rho_l = \rho_+$ if $\rho > \rho^*$. In TASEP, this change of the reservoir density is reflected by different insertion rates $\alpha_- = \rho_-$ and $\alpha_+ = \rho_+$. The same scenario can be transferred from the viewpoint of individual drivers to the viewpoint of a traffic-management center that tries to control the density in the system in order, for example, to maximize the flow. At both ends of the road section there might be sensors that count entering and leaving cars and the controller is able to change the inflow if a certain number of cars is exceeded. Obviously if one does not control the outflow from the bottleneck as well, one will not generally be able to keep a desired density in the system. However, it is interesting to decide whether this incomplete regulation can be appropriate for real traffic situations in certain parameter regions. The scenario can be interpreted as a sort of ramp metering and reflects a common way of flow maximization in practice [15–17]. One way to reduce the time-averaged inflow is by a traffic light that switches the effective left-reservoir density to zero from time to time [7,18,19]. Another possible application of this varying input rate is the concept of dynamic toll: At the entrance (which plays the roll of a toll booth) a prize for passing the road section is computed in dependence of the current occupation of vehicles [13,20,21]. While those problems are specially dedicated to traffic, the considerations of the present paper are quite general so results apply not only to traffic but also to other transport scenarios far from equilibrium (see Ref. [6] for an overview of applications in other research areas as intracellular transport) with density-feedback control as well.

*marko.woelki@dlr.de

 ©2013 American Physical Society

The remainder of the paper is as follows. In Sec. II, we define the TASEP with density-feedback control (DFC) that generalizes the particle-insertion procedure of the usual TASEP. We continue by deriving its mean-field equations from the Burgers equation with the modified boundary condition. The following Sec. III presents analytical results from numerical solutions of the mean-field equations. Special interest is given to the phase diagram of the TASEP influenced by DFC. Section IV shows how DFC can be used for flow optimization in TASEP and highlights the benefit of DFC in contrast to the generic TASEP. In Sec. V computer simulations of TASEP with DFC are presented and compared to the analytical predictions before we formulate our conclusions.

II. MODEL DEFINITIONS

First, the mechanism of density-feedback control is defined from the microscopic and macroscopic viewpoints and how they translate into each other is discussed.

A. Density-feedback control TASEP

The microscopic TASEP model is defined on a one-dimensional lattice with L sites, labeled from left to right as $l = 1, 2, \ldots, L$. Each site is either occupied by a single particle or is empty; this defines its time-dependent states, $\tau_l(t) = 1$ (occupied) and $\tau_l(t) = 0$ (empty). Particles whose right neighboring site is vacant may move onto this site at rate p. From the last site a particle leaves the system at constant rate β, while particles enter the system on site 1 at rate α. The process is considered in continuous time, where we can set the time scale by taking $p = 1$. In the following we consider the TASEP with DFC, which implies modified particle insertion as follows:

$$\alpha(N) = \begin{cases} \alpha_-, & \text{for} \quad N < N^* \\ \alpha_+, & \text{for} \quad N \geqslant N^* \end{cases}. \tag{1}$$

Hence, the probability that a particle enters the lattice at site 1 takes a different value if the actual particle number N is above or below a threshold N^*.

We note certain limits of this process: if $\rho^* = 0$ ($\rho^* = 1$) one recovers the TASEP with $\alpha = \alpha_+$ ($\alpha = \alpha_-$). If we take $\alpha_+ = 0$ the process is very related to the works of Refs. [9–11]. In those works, however, the TASEP is considered with a constrain on the overall particle number, including the single reservoir from which particles are injected and to which particles leave the lattice.

B. Burgers equation approach

The starting point for the macroscopic description is the viscous Burgers equation,

$$\frac{\partial \rho}{\partial t} + \frac{\partial[\rho(1-\rho)]}{\partial x} = D\frac{\partial^2 \rho}{\partial x^2}, \tag{2}$$

for the density $\rho = \rho(x,t)$ with the right boundary condition $x(L,t) = \rho_r$. Instead of the generic left-hand boundary condition

$$\rho(0,t) = \rho_l, \tag{3}$$

we use a dynamical density $\rho_l(t)$ that depends on the (spatially) averaged density $\bar{\rho}(t)$ at time t as

$$\rho_l(t) = \begin{cases} \rho_-, & \text{for} \quad \bar{\rho}(t) < \rho^* \\ \rho_+, & \text{for} \quad \bar{\rho}(t) \geqslant \rho^* \end{cases}. \tag{4}$$

Here ρ^* is a limiting density beyond which ρ_l is reduced in order to control the average density $\bar{\rho}$. Note that all densities are normalized to remain in the interval [0; 1]. For numerical simulations we chose an initial linear profile $\rho(x,0) = (\rho_r - \rho_-)x/L + \rho_-$ and let the system evolve into the steady state. We emphasize that the phase boundary between the HD_+ and HD_- phases depends on the initial condition.

The numerical results for the Burgers equation are obtained by spacial discretization. This leads to [7]

$$\frac{\partial}{\partial t}\rho_i = -(1-2\rho_i)\frac{\rho_{i+1} - \rho_{i-1}}{2} + D(\rho_{i+1} + \rho_{i-1} - 2\rho_i). \tag{5}$$

In the remainder of the paper the diffusion constant is set to $D = 1/2$. This equation then turns into

$$\frac{\partial \rho_i}{\partial t} = \rho_{i-1}(1-\rho_i) - \rho_i(1-\rho_{i+1}), \tag{6}$$

which is nothing but the mean-field equation for the microscopic dynamics of the TASEP. The following section presents the results from numerical solutions of those mean-field equations.

III. ANALYTIC RESULTS

The mean-field theory assumes that correlations between neighboring sites vanish, so the probability to find a certain lattice configuration factorizes into simple on-site factors, namely ρ_i if site i is occupied and $1 - \rho_i$ if site i is empty; compare [6]. In the present realization the boundary conditions are $\rho_{L+1} = \rho_r = \text{const}$ and

$$\rho_0 = \rho_l = \begin{cases} \rho_-, & \text{for} \quad \bar{\rho} < \rho^*, \\ \rho_+, & \text{for} \quad \bar{\rho} \geqslant \rho^*, \end{cases} \quad \text{with} \quad \bar{\rho} = \frac{1}{L}\sum_{i=1}^{L}\rho_i. \tag{7}$$

Further,

$$\rho_1(1-\rho_2) = \rho_l(1-\rho_1) \quad \text{and} \quad (1-\rho_r)\rho_L = \rho_{L-1}(1-\rho_L). \tag{8}$$

The general solution for $1 < i < L$ is [22]

$$\rho_i = \frac{-\rho_s\rho_u\left(\rho_s^{i-1} - \rho_u^{i-1}\right) + \left(\rho_s^{i} - \rho_u^{i}\right)\rho_1}{-\rho_s\rho_u\left(\rho_s^{i-2} - \rho_u^{i-2}\right) + \left(\rho_s^{i-1} - \rho_u^{i-1}\right)\rho_1}. \tag{9}$$

Here ρ_s and ρ_u are the solutions of $J = \rho(1-\rho)$. From Fig. 1(a) we can identify the well-known phases: low-density (LD) phase: $\bar{\rho} = \rho_l$ for $1 - \rho_r > \rho_l$ and $\rho_l < 1/2$; high-density (HD) phase: $\bar{\rho} = \rho_r$ for $1 - \rho_r > \rho_l$ and $1 - \rho_r < 1/2$; and maximum-current (MC) phase: $\bar{\rho} = \frac{1}{2}$ for $\rho_l, 1 - \rho_r > 1/2$. Now we investigate the new boundary condition (4). Table I shows the phases that can be identified.

Before we turn into details, we emphasize that the various phases in Table I indicated by $-$ and $+$ are coupled effectively by either of the left reservoirs at densities ρ_- and ρ_+,

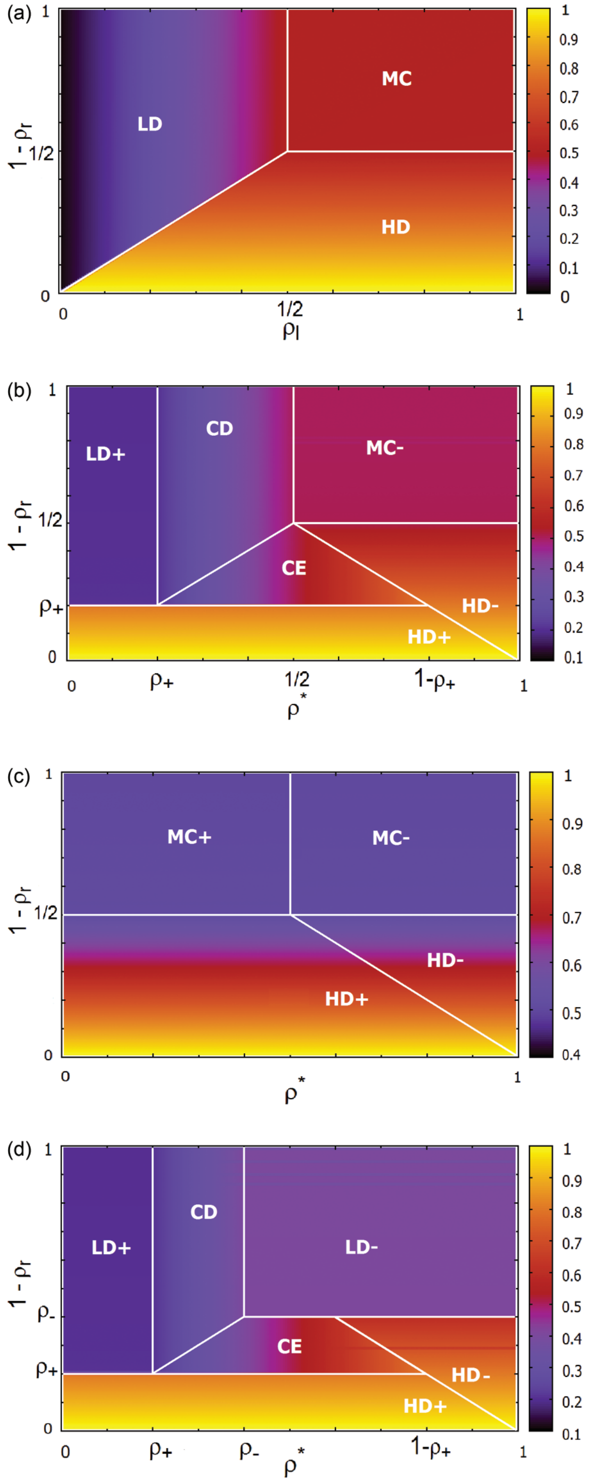

FIG. 1. (Color online) Phase diagrams. (a) Generic left boundary condition (3) corresponding to $\rho_- = \rho_+ = \rho_l$ and below (b)–(d) for the dynamic boundary condition (4). The coloring encodes the value of the average density $\bar{\rho}$. (b) $\alpha_- = 0.6$ and $\alpha_+ = 0.2$ so $\rho_+ < 1/2 < \rho_-$; (c) $\alpha_- = 0.8$ and $\alpha_+ = 0.6$ $(1/2 < \rho_+ < \rho_-)$; (d) $\alpha_- = 0.4$ and $\alpha_+ = 0.2$ $(\rho_+ < \rho_- < 1/2)$.

respectively. Additionally, two phases are observed that are completely new compared to the generic TASEP; see Table I. Those are the controlled-density (CD) phase and the coexistence (CE) phase. Figure 2 shows typical density profiles

TABLE I. Average left-hand and overall density in the various phases.

Phase	ρ_l^{eff}	$\bar{\rho}$
Low-density (LD$_+$)	ρ_+	ρ_+
Low-density (LD$_-$)	ρ_-	ρ_-
High-density (HD$_+$)	ρ_+	ρ_r
High-density (HD$_-$)	ρ_-	ρ_r
Maximum-current (MC$_-$)	ρ_-	$1/2$
Maximum-current (MC$_+$)	ρ_+	$1/2$
Controlled-density (CD)	ρ^*	ρ^*
Coexistence (CE) phase	$1 - \rho_r$	ρ^*

of those phases. One sees that the CE phase exhibits a stable upward shock that separates a high-density region and a low-density region. In both phases the system is not dominated by contact with either of the two left reservoirs but both reservoirs are coupled in rapid alternation to the system. Summarizing, the stationary system behaves as if it would be coupled to an effective left boundary reservoir with constant density ρ_l^{eff} that differs from phase to phase; see Table I. In each phase, it is helpful to have in mind where on the horizontal axis of the generic phase diagram from Fig. 1(a) the values of ρ_-, ρ_+, and ρ_l^{eff} locate. One then can imagine in each case which phases are reached by variation of ρ_r, i.e., by moving vertically through the generic phase diagram. The reader shall imagine those vertical lines for ρ_- and ρ_+ in order to understand phenomenologically the value of ρ_l^{eff} in the different cases shown in Fig. 1(b)–1(d) that are explained in the following. We begin with Fig. 1(c): If both ρ_+ and ρ_- exceed 1/2, both those lines cross the MC-HD transition line. In both cases, MC and HD phases appear for $1 - \rho_r$ greater or smaller than $1/2$, respectively. In the MC phase, for $\rho^* < 1/2$ $(\rho^* > 1/2)$, the average density $\bar{\rho} = 1/2$ is smaller (greater) than ρ^*. Therefore ρ_l^{eff} equals ρ_+ (ρ_-) for $\rho^* < 1/2$ $(\rho^* > 1/2)$ and the MC phase is distinguished in MC$_+$ and MC$_-$. Also the HD phase is distinguished further: Both (sub-)phases are separated by

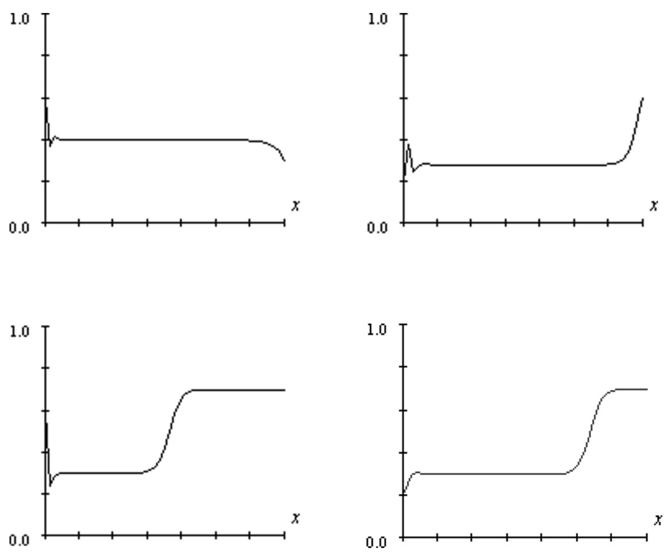

FIG. 2. Density profiles for typical values of ρ_l and ρ_r. Top figures: CD phase; bottom figures: CE phase.

the line $\rho_r = \rho^*$. Since ρ_r is the bulk density, in the region $\rho_r < \rho^*$ one finds $\rho_l^{\text{eff}} = \rho_-$ with the help of (4). Therefore, this is the HD$_-$ phase. Similar arguments hold for the HD$_+$ phase.

If $\rho_+ < 1/2$ and $\rho_- > 1/2$, one arrives at the phase diagram in Fig. 1(b). The location of the LD$_+$ phase is explained as follows: First, from the TASEP phase diagram Fig. 1(a) it is known that a low-density state is reached for $1-\rho_r > \rho_l$; second, if $\rho^* < \rho_+$ then it is evident from (4) that the system behaves as if there would be a left boundary reservoir with density $\rho_l^{\text{eff}} = \rho_+$. In case of Fig. 1(b) only ρ_- is large enough to lead to an MC phase. Hence, the occurring phase has $\rho_l^{\text{eff}} = \rho_-$ and is referred to as the MC$_-$ phase. The imaginary vertical line ρ_+ in Fig. 1(a) crosses the coexistence line between the high- and low-density phases where $\rho_l = 1-\rho_r$ in the generic TASEP. This crossing leads to the CE phase, consequently, with $\rho_l^{\text{eff}} = 1-\rho_r$. The CD phase is in fact a low-density phase with $\rho_l^{\text{eff}} = \rho^*$, appearing here for $\rho_+ < \rho^* < 1/2$. What happens is quite intuitive: The system is equilibrated at the left end due to permanent change of contact with reservoir densities ρ_+ and ρ_- around the control value ρ^*. In the same way one can explain the phase diagram Fig. 1(a). Regarding the appearance of the LD$_-$ phase, if $\rho^* > \rho_-$, it is expected with (4) that the average density becomes ρ_- and the system remains in contact with the ρ_- reservoir. Finally, we stress that the bulk density $\bar{\rho}$, given in Table I, can be deduced from the maximum-current principle [6,7] which takes here the form

$$J = \bar{\rho}(1-\bar{\rho}) = \begin{cases} \min_{[\rho_l^{\text{eff}},\rho_r]}\rho(1-\rho), & \text{if} \quad \rho_l^{\text{eff}} < \rho_r \\ \max_{[\rho_l^{\text{eff}},\rho_r]}\rho(1-\rho), & \text{if} \quad \rho_l^{\text{eff}} > \rho_r \end{cases}. \tag{10}$$

In the CE phase one finds coexistence of an HD phase at density ρ_r and a CD phase at density $1-\rho_r$. Where both regions merge a shock is formed; see Fig. 2. Since the average density remains $\bar{\rho}$ the position x_s of the shock is given by $\rho^* = (1-\rho_r)x_s + \rho_r(L-x_s)$. The phase diagram as depicted in Fig. 1(b) obviously holds only if we take $\rho_- > 1/2$ and $\rho_+ < 1/2$. If both values exceed 1/2 the system is in HD phases for $\rho_r > 1/2$ and MC phases otherwise [23]. If both ρ_+ and ρ_- have values below 1/2, then obviously MC phases are suppressed. The results are shown in Fig. 1(c) and 1(d).

IV. FLOW OPTIMIZATION BY DFC

A. Optimal choice of ρ^*

The phase diagram of the TASEP with DFC (see Fig. 1) and the values of $\bar{\rho}$ in the various phases (see Table I) give an idea how to set the threshold ρ^* in order to keep the flow as large as possible. One can think of α_- being given by the (constant) demand of incoming drivers and β being given by the characteristics of the outflow region of the bottleneck. We consider the scenario of Fig. 1(b) and, thus, argue from the viewpoint of the mean-field description. We move through the phase diagram on a virtual horizontal line for constant β. Here one can distinguish the following three cases: The bulk density starts at α_+ and then takes the value of ρ^* and increases until it reaches the value of 1/2 (case 1: for $1/2 < \beta < 1$) or $1-\beta$ (case 2: for $\alpha_+ < \beta < 1/2$). In case 3 (for $0 < \beta < \alpha_+$) the bulk density remains at $1-\beta$ for all choices of the threshold ρ^*. From a traffic viewpoint, the interest is in maximizing the flow. The closer the density is to 1/2, the higher the flow becomes, due to the relation $J = \rho(1-\rho)$. Thus, in case 1 the flow is maximized for $\rho^* \geqslant 1/2$ and in case 2 for exactly 1/2 (in case 3, remember, it is independent of ρ^*). Now consider Fig. 1(c). In case 1 the flow is maximized for $\rho^* \geqslant \rho_r$ $(= 1-\beta)$ and in case 2 for $\rho^* = 1/2$. Finally, consider Fig. 1(d). For $\beta > 1/2$ $(\beta < 1/2)$ the flow is independent of ρ^* equal to 1/2 $[\beta(1-\beta)]$. Thus, concluding, one can say that the choice $\rho^* = 1/2$ theoretically is always the best in order to maximize the flow. This result is expected since this is the density at which the flow has its maximum. Therefore, in the following we restrict ourselves to this case, noting that results easily convert to the general case.

B. Benefit by DFC

Figure 3 illustrates the benefit of DFC. The dashed red (continuous green) objects correspond to the case where $\rho_- > 1/2$ $(\rho_- < 1/2)$. In Fig. 3(a) we draw an analogy to the generic system in assuming that ρ_- corresponds to the generic left reservoir density. The figure then shows that the switching to a lower density ρ_+ leads to a conversion of a high density to density 1/2. Figure 3(b) shows the benefit of DFC in the

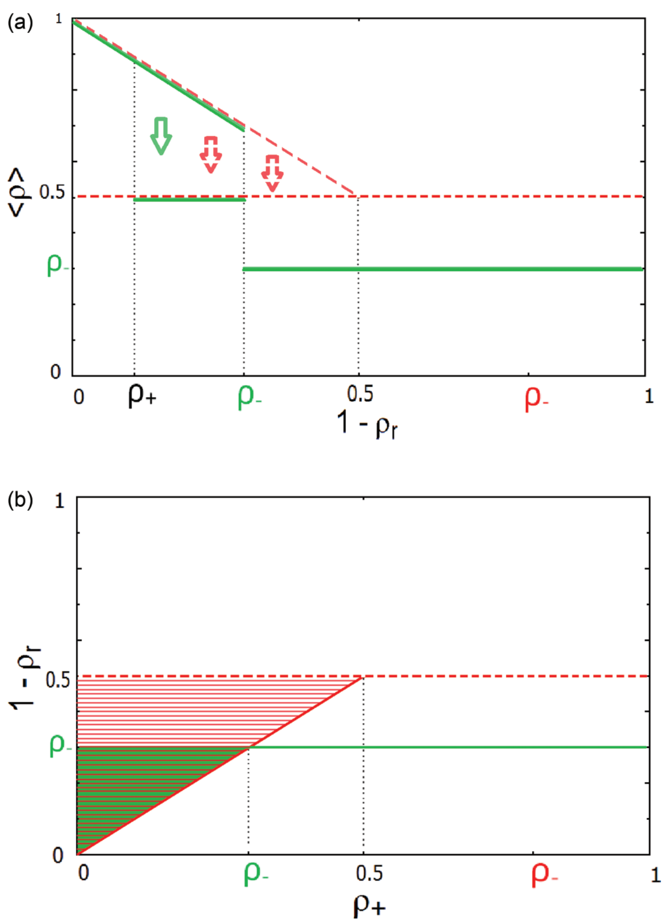

FIG. 3. (Color online) (a) Optimization of density and flow by conversion of high density into density 1/2 by DFC. (b) Phase diagram showing the benefit of DFC. The dashed red (continuous green) triangle is the region that is optimized to a maximum-current region by density-feedback control for $\rho_- > 1/2$ $(\rho_- < 1/2)$.

(ρ_+,β) plane. For simplicity we write β instead of $1-\rho_r$. One sees the according additional triangular MC region belonging to this benefit.

Above the dashed line (and $\rho_- > 1/2$) the system is in the MC phase. The outflow is high enough ($\beta > 1/2$) to suppress HD phases and therefore no optimization is possible there. Similarly, above the continuous line (and $\rho_- < 1/2$) the system is in the LD phase where the density is smaller than $1/2$. Since DFC can only lower the density, the flow can never be optimized. To the right of the triangles ($\rho_+ > \beta$) and below the line ($\beta < 1/2$ or $\beta < \rho_-$, respectively) one finds the HD phase. Since both ρ_- and ρ_+ are larger than β, the inflow is always higher than the outflow and the high-density phase cannot be left by variation of ρ_+.

V. SIMULATION RESULTS

We repeat that the results of Sec. III are exact consequences of the discretized Burgers equation (6); however, they will, in general, not be exact for the corresponding TASEP with DFC, since the latter is described by (6) on a mean-field level. The weakness of the mean-field approach is that it ignores correlations arising from spatial inhomogeneities, including the existence of boundaries. However, for the quantity of interest, namely the average density at threshold $\rho^* = 0.5$, results will turn out to be in good agreement.

A. Simulation of the TASEP with DFC

Figure 4 shows space-time plots with increasing space coordinates in the right direction and time increasing in the downwards direction. Standing particles that entered at densities lower than ρ^* are in red (gray) while standing particles that entered at higher densities are in black. Plotted are only those time steps where a move occurs; for the moving particle there is an additional color that is not important.

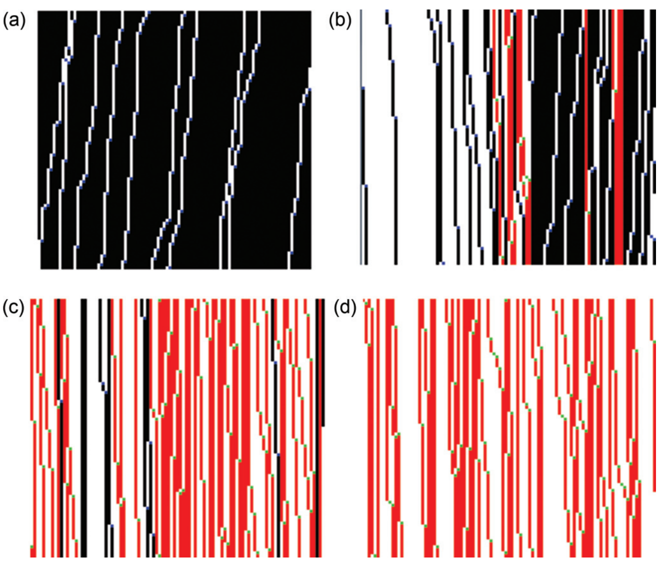

FIG. 4. (Color online) Space-time plots for $\rho^* = 0.5$ in a system with 100 cells. In panels (a), (b), and (c): $\alpha_- = 0.6$, $\alpha_+ = 0.2$, and $\beta = 0.1$. [(a) HD$_+$ phase] $\beta = 0.3$, [(b) CE phase] $\beta = 0.6$, (c) MC$_-$ phase (transition line to CD phase). $\alpha_- = 0.4$, $\alpha_+ = 0.2$, $\beta = 0.6$ in [(d) LD$_-$ phase].

In order to average quantities in the steady state, it turns out that the simulation of the TASEP with DFC converges very slowly. Therefore, as in Refs. [9–11], it was chosen to feed the simulation at the expected density. For our studies, thus, the mean-field density serves as initial value. During 2×10^6 time steps the system is let alone and afterwards every 100 time steps the density is measured over 5×10^6 steps. The average over the steady states of 100 different initial configurations was taken.

B. Comparison with the mean field

First, we will verify that the different phases resulting from the mean-field theory indeed occur in the TASEP with DFC and that the physics is correctly predicted. Figure 5(a) shows the simulated density profiles that correspond to the space-time plots of Fig. 4: The green circles saturating at density 0.9 show the HD profile of Fig. 4(a) and reproduce the mean-field density ρ_r of HD phases. The profile of red squares corresponds to the CE phase of Fig. 4(b) and clearly shows the coexistence of low and high densities so the existence of the shock phase in the TASEP with DFC is verified. The profile corresponding to Fig. 4(c) on the transition line between CD and MC is given by the blue diamonds showing the flat profile around density $1/2$, which is the average density predicted by

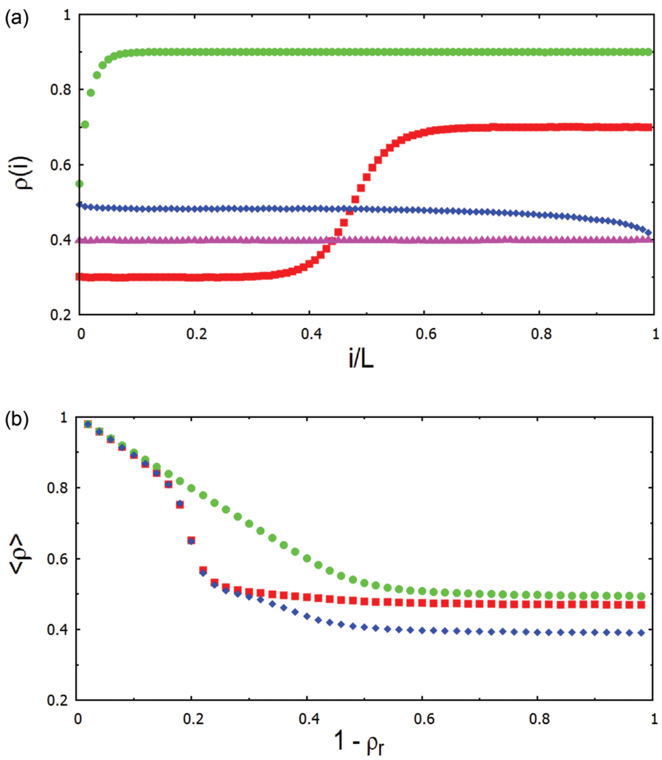

FIG. 5. (Color online) The figures show simulation results in case of $\rho^* = 0.5$ for a system of length . (a) Density profiles corresponding to Fig. 4. (b) Average density versus β. Red squares belong to $\rho_+ = 0.2$ and $\rho_- = 0.6$ [parameter case as in Fig. 1(b)], green circles correspond to $\rho_+ = 0.6$ and $\rho_- = 0.8$ [parameter case as Fig. 1(c)], and blue diamonds correspond to $\rho_+ = 0.2$ and $\rho_- = 0.4$ [parameter case as Fig. 1(d)].

the mean field. Finally, the situation shown in Fig. 4(d) has a flat profile with a constant density of 0.4. Note that in this case ($\rho_l^{\mathrm{eff}} = 1 - \rho_r$) the mean-field becomes exact.

Now we turn to the simulation of the average density in the system against β in order to verify that densities and phase boundaries are correctly predicted. The results are shown in Fig. 5(b). See the figure caption for more details. One sees that the green circles are on the line $\rho = \rho_r$ for $\beta < 0.5$ and that $\rho = 0.5$ for $\beta \geqslant 0.5$ (which corresponds to the transition from HD to MC) as predicted by the mean field. The red squares start in HD and clearly jump at $\rho_+ = 0.2$ to density $1/2$ (corresponding to CE and MC). The blue diamonds clearly show three phases [as can be seen from Fig. 1(d)]. Starting at HD one sees the kink at $\beta = \rho_+$ to the CE phase and another transition at $\beta = \rho_-$ to MC and $\rho = 1/2$, which is also in agreement with our mean-field predictions. Of course, the sharpness of the transitions could be ameliorated by taking larger system sizes.

VI. CONCLUSION

This paper studied a bottleneck situation of traffic with inflow at the left and outflow at the right end which was modeled by TASEP and the Burgers equation. For this situation, a concept to control the overall density has been analyzed. The left reservoir density takes the form $\rho_l(\bar{\rho}(t))$ and, thus, depends on the density at time t, generalizing the generic constant left reservoir density. It is reduced from ρ_- to ρ_+ if the spatially averaged density $\bar{\rho}(t)$ at time t lies above a certain threshold ρ^*. In contrast, the right end is kept in contact to a reservoir at fixed density ρ_r. The mechanism is referred to as DFC. The same mechanism is provided in everyday life, where cars enter a dense road section at a smaller rate when there are possible alternatives. The paper showed that DFC can be efficiently used to maximize the flow by converting a fraction of the high-density phase to a maximum-current phase.

From numerical solution of the discretized Burgers equation the phase diagram in the plane spanned by ρ^* and $1 - \rho_r$ was derived that showed a rich phase behavior. The process exhibits two low-density, high-density, and maximum-current phases that correspond to the two left boundary reservoirs. In addition, there is a phase in which high and low density coexist so a macroscopic shock profile can be observed. This phase corresponds to the coexistence line in the generic model between the low- and high-density phases. There also is a phase that is completely new compared to the generic model but can be anticipated intuitively; in this phase, the repeated change of the left-hand reservoir density around the threshold ρ^* leads to an effective density ρ^*. It was further investigated for which choice of ρ^* the flow is maximized. It could be shown that, although in the generic TASEP the flow is monotonically increasing with the left reservoir density, DFC optimizes the flow if the threshold density is chosen appropriately.

For the optimal choice of the threshold ($\rho^* = 1/2$), we verified, with the help of Monte Carlo simulations, that the mean field correctly predicts the average density (and therewith the flow) in the system as well as the physics of the various phases, including the coexistence phase. Note that simulations in which the Heaviside dependence of the density was replaced by a hyperbolic tangent with appropriate sharpness, inspired by Ref. [9], have also been performed. This takes into account a (realistic) delay of the adjustment of the left density through feedback control. Further, the model with parallel dynamics has been considered [24]. It turned out that results agree very much with the continuous-time case studied here. Further investigations could focus on the Nagel-Schreckenberg model of traffic flow. It is known that the phase diagram of the Nagel-Schreckenberg model remains even for larger maximum velocity [18] (where cars can move more than a single site per time step). While in the present model flow optimization is achieved at a threshold density $1/2$ one should decide whether this generalizes to the density at which the flow becomes maximal (as one would expect [17]). The next step is a generalization to more realistic microscopic traffic models, as, for example, the Krauß model [25], in order to study effective traffic-management strategies based on DFC.

ACKNOWLEDGMENTS

The author thanks Peter Wagner for helpful comments.

2 [1] K. Mallick, Proceedings of the STATPHYS24 conference, arXiv:1101.2849 (2011).

[2] K. Nagel and M. Schreckenberg, J. Phys. I (France) **2**, 2221 (1992).

[3] M. J. Lighthill and G. B. Witham, Proc. R. Soc. London, Ser. A **229**, 317 (1955).

Q [4] K. Nagel, Phys. Rev. E **53**, 4655 (1996).

[5] D. Helbing, Rev. Mod. Phys. **73**, 1067 (2001).

[6] R. A. Blythe and M. R. Evans, J. Phys. A **40**, R333 (2007).

[7] V. Popkov, M. Salerno, G. M. Schutz, Phys. Rev. E **78**, 011122 (2008).

[8] A. J. Wood, J. Phys. A **42**, 445002 (2009).

3 [9] D. A. Adams, B. Schmittmann, and R. K. P. Zia, J. Stat. Mech. (2007) P06009.

[10] L. J. Cook and R. K. P. Zia, J. Stat. Mech. (2009) P02012.

[11] L. J. Cook and R. K. P. Zia, J. Stat. Mech. (2010) P07014.

[12] L. J. Cook and R. K. P. Zia, J. Stat. Mech. (2012) P05008. Q

[13] Fosgerau, Mogens: How a fast lane may replace a congestion toll, DTU Transport, p. 15 (2011).

[14] J. Brankov, N. Pesheva, and N. Bunzarova, In: *Proceedings of the X Jubilee National Congress on Theoretical and Applied Mechanics, Varna, 13–16 September, 2005*, pp. 442–456 arXiv:0803.2625 [cond-mat.stat-mech] (2006). 4

[15] B. S. Kerner, J. IEEE Transact. Intelligent Transport. Syst. **8**, 308 (2007).

[16] D. Helbing, Europhys. Lett. **47**, 196 (1999).

[17] E. Smaragdis, M. Papageorgiou, and E. Kosmatopoulos, Transport. Res. B **38**, 251 (2004).

[18] R. Barlovic, T. Huisinga, A. Schadschneider, M. Schreckenberg, Phys. Rev. E **66**, 046113 (2002).

[19] T. Neumann, Eur. Phys. J. B **67**, 133 (2009).

[20] A. Bhargava, E. A. Oware, S. Labi, and K. C. Sinha, Ramp Metering and High Occupancy Vehicle Facilities: A Synthesis Study. Publication FHWA/IN/JTRP-2006/02. Joint Transportation Research Program, Indiana Department of Transportation and Purdue University, West Lafayette, Indiana
5 (2006).

[21] A. D. Spiliopoulou, I. Papamichail, and M. Papageorgiou, ASCE J. Transport. Eng. **136**, 67 (2010).

[22] B. Derrida, E. Domany, and D. Mukamel, J. Stat. Phys. **69**, 667 (1992).

[23] Note that one special case that has completely different physics is excluded here: $\rho_- < \rho_+$.

[24] M. Woelki (unpublished). 6

[25] S. Krauss, P. Wagner, and C. Gawron, Phys. Rev. E **55**, 5597 (1997).